

# Overcharging of DNA in the presence of salt: Theory and Simulation

Markus Deserno,<sup>1,2</sup> Felipe Jiménez-Ángeles,<sup>3,4</sup> Christian Holm,<sup>1</sup> and Marcelo Lozada-Cassou<sup>3,4</sup>

<sup>1</sup>*Max-Planck-Institut für Polymerforschung Ackermannweg 10, 55128 Mainz, Germany*

<sup>2</sup>*Department of Chemistry and Biochemistry UCLA,  
405 Hilgard Avenue, Los Angeles CA 90095, USA*

<sup>3</sup>*Programa de Ingeniería Molecular, Instituto Mexicano del Petróleo,  
Lázaro Cárdenas 152, 07730 México, D. F., México*

<sup>4</sup>*Departamento de Física, Universidad Autónoma Metropolitana-Iztapalapa,  
Apartado Postal 55-334, 09340 D.F. México*

(Dated: November 5, 2018)

A study of a model rod-like polyelectrolyte molecule immersed into a monovalent or divalent electrolyte is presented. Results for the local concentration profile, mean electrostatic potential, charge distribution function and  $\zeta$ -potential are obtained from hypernetted-chain/mean spherical approximation (HNC/MSA) theory and compared with molecular dynamics (MD) simulations. As a particular case, the parameters of the polyelectrolyte molecule are mapped to those of a DNA molecule. Both, HNC/MSA and MD, predict the occurrence of overcharging, which is not present in the Poisson-Boltzmann theory. Further an excellent qualitative, and in some cases quantitative, agreement between HNC/MSA and MD is found. Oscillations observed in the mean electrostatic potential, local concentration profiles, as well as the curvature of the  $\zeta$ -potential are discussed in terms of the observed overcharging effect. Particularly interesting results are a very non-monotonic behavior of the  $\zeta$ -potential, as a function of the rod charge density, and the overcharging by *monovalent* counterions.

PACS numbers:

## INTRODUCTION

“Polyelectrolytes are polymers bearing ionizable groups, which, in polar solvents, can dissociate into charged polymer chains (macroions) and small counterions” [1]. The combination of macromolecular properties and long-range electrostatic interactions results in an impressive variety of phenomena. It makes these systems interesting from a fundamental as well as a technological point of view. A thorough understanding of polyelectrolytes has become increasingly important in biochemistry and molecular biology. This is due to the fact that virtually all proteins, as well as the DNA, are polyelectrolytes. Their interactions with each other and with the charged cell-membrane are still far from being fully understood, which is partly due to the intricate coupling between ion distribution and chain conformation.

A first approach to the problem is to fix the conformation of the chain and to focus on a detailed description of the counterion distribution. Usually polyelectrolytes stretch due to the electrostatic repulsion of their charged groups. Moreover, many important polyelectrolytes have a large intrinsic stiffness (e.g., DNA, actin filaments or microtubules). Therefore, a rod-like conformation is an obvious first choice. The remaining problem of charged rods immersed into solution is much easier, but is still far from being exactly solvable.

An additional approximation, which is frequently used in theoretical descriptions, is to completely integrate out the counterionic degrees of freedom. On a linearized

mean-field level this yields a Debye-Hückel-like theory characterized by a screened Coulomb potential between charged monomers. To obtain the correct physical properties, one uses an *effective* Yukawa potential, which in turn requires adjustable parameters such as an effective polyelectrolyte radius and charge. In this way the dependence of the ionic structure, hereafter called electrical double layer (EDL), around two or more polyelectrolytes, as a function of the polyelectrolyte-polyelectrolyte distance, is not accounted for. This information, however, is most relevant for the understanding of polyelectrolyte aggregation or self-assembling. This effect is more important for polyelectrolytes in low concentration added salt solution, since for this case the ionic screening is weak. This has been shown to be relevant for charged plates and charged spherical macroions [2, 3, 4].

A common further approximation assumes that the investigation of a small sub-volume containing only one rod and its counterions will suffice to unveil much of the interesting physics. The main justification for this approach is that the sub-volume has zero net charge. Moreover, the counterions will also efficiently screen higher order multipoles. Hence, the interactions between two such sub-volumes, which are neglected when focusing on just one rod, will be fairly weak. This approximation is called cylindrical cell model and it provides the framework for our simulation calculation.

One attractive feature of the cell model is that in the salt-free case the nonlinear PB equation can be solved *exactly* in this geometry [5, 6]. It also displays in a

clear fashion the effect of partial counterion *condensation* [7, 8]. While a charged sphere loses all its counterions upon dilution, a charged plane keeps all of them. For a charged cylinder the fraction of ions, which upon dilution remain in the vicinity of the macroion, can be anywhere between 0 and 100%. Addition of salt increases the screening of the charged rod. If the salt content is large enough, the electric field will have decayed to zero before the cell radius is reached. It is then permissible to extend the latter to infinity. This is the approach that we use for our integral equation calculations.

The PB theory shows its limitations for systems where ion correlations become important [9]. It cannot predict the attractive forces which are seen experimentally in DNA solutions [10] and which have been also found in various simulation [11, 12, 13] and integral equation [14, 15, 16] studies in the presence of multivalent counterions.

In this paper we present studies for a rod immersed in a salt solution which PB theory fails to describe correctly, namely, the possibility of overcharging a single rod, resulting in an effective charge reversal, and the appearance of a non-monotonic zeta-potential [17, 18, 19]. This effect is most relevant in electrophoresis experiments [20]. The overcharging of a macroion modifies in a non-linear fashion the electrophoretic mobility as a function of the polyelectrolyte charge and salt concentration. In the classical electrophoresis theory of Wiersema, O'Brien and White [21, 22], which is a linear theory based on the Poisson-Boltzmann (PB) description of the EDL around the polyelectrolyte, this effect is not included.

The EDL obtained through the well established integral equation approach does predict overcharging [17, 18]. The overcharging effect has been observed in Monte Carlo (MC) simulations for planar [23], cylindrical [24] and spherical [25, 26] geometries. Moreover, several years ago, Gonzales-Tovar *et al.*[18] predicted that for some macroion charge and electrolyte concentration the overcharging produces an electrophoresis mobility reversal. This mobility reversal has been experimentally observed [27, 28, 29, 30]. This effect has been taken into account in the electrophoresis theory by Lozada-Cassou *et al.*[31]. An excellent qualitative agreement with experimental results [20, 28, 30] is found. This overcharging effect and the predicted mobility reversal have been recently addressed by Deserno *et al.*[9] and Shklovskii [32, 33].

In Ref. [9] ion distributions are studied via the integrated charge distribution function,  $P(r)$ , and overcharging is addressed based on MD simulations. In the present paper we extend this research by approaching the overcharging effect through a well established integral equation theory [17, 18] as well as more detailed molecular dynamics (MD) simulations. We compute  $P(r)$ , the concentration profiles  $g_i(r)$ , the mean electrostatic potential profile  $\psi(r)$ , and the  $\zeta$ -potential. A comparison of the integral equation results with those from MD is presented.

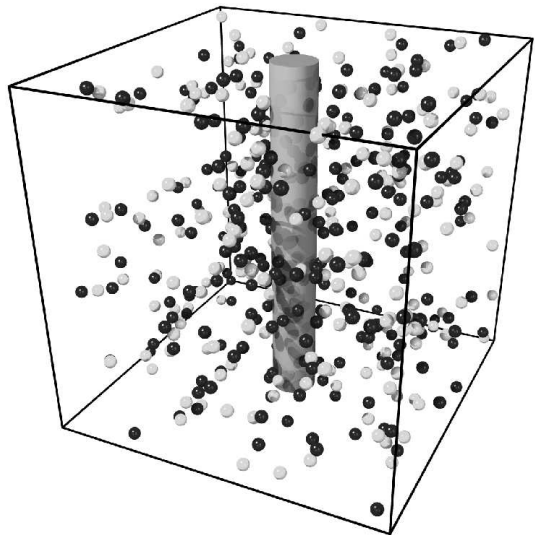


FIG. 1: Realization of the cell model. A rod of length  $L_b$  placed parallel to an edge of a cube of side length  $L_b$  yields an infinite square array of infinitely long rods upon periodic replication of the cubic box. The dark particles are the counterions or positive salt ions and the bright particles are the negative salt ions. This particular snapshot contains 36 divalent counterions, 220 positive and 220 negative divalent salt ions.

## SIMULATIONAL DETAILS OF THE MODEL SYSTEM

### Generating a cell-geometry

Compared to the spherical cell model, the cylindrical one presents one additional but crucial complication: the charged rod is infinitely long. Several methods have been proposed in the literature to handle this problem. They essentially all use as a unit cell a hexagonal prism with a certain height. This approximates the cylindrical cell by the “most round” space-filling object. In this publication we take a computationally even simpler approach by using a *cubic* unit box of side-length  $L_b$  and placing the DNA parallel to one of the edges (see Fig. 1). The justification for this approach is as follows: In a high-salt environment the charged rod will be screened within a distance much smaller than the size of the box. The potential will therefore become constant long before the deviations from a cylindrical cell will be felt. It is thus largely irrelevant, whether these deviations are of hexagonal or of cubic type. When comparing with the cylindrical cell model, a radius  $R = L_b/\sqrt{\pi}$  is appropriate, since it yields the same area per rod.

The main advantage of this approach is that such a system can be treated with the plain cubic Ewald sum or one of its mesh-upgrades [34, 35, 36, 37]. This permits a very efficient way for computing the long-range electrostatic interactions.

## Interaction potentials and DNA mapping

A specification of two interaction potentials is necessary to describe the model system: *(i)* an excluded volume interaction preventing two particles from occupying the same position in space and *(ii)* the long-range Coulomb potential.

For the excluded volume interaction between the ions we use the following potential:

$$V_{\text{ion-ion}}^*(r) = \begin{cases} 4\epsilon \left[ \left(\frac{a}{r}\right)^{12} - \left(\frac{a}{r}\right)^6 + \frac{1}{4} \right] & : 0 < r \leq r_{\text{cut}} \\ 0 & : r_{\text{cut}} < r. \end{cases} \quad (1)$$

Without the cutoff this would be the common Lennard-Jones potential describing particles with a diameter  $a$  and an attractive potential minimum of  $\epsilon$ . In order to achieve pure repulsion, we cut the potential at the minimum and shift it up such that it smoothly goes to zero there. As a consequence,  $\epsilon$  becomes largely irrelevant. Since two ions a distance  $a$  apart have the (repulsive) interaction energy  $\epsilon$ , we make the natural choice  $\epsilon = k_{\text{B}}T$ .

In order to give the rod a larger radius than the ions, we employ an ion-rod potential similar to Eq. (1), in which  $r$  is replaced by  $r - r_{\text{s}}$ . This shifts the hard core a distance  $r_{\text{s}}$  towards larger radii and gives a distance of closest approach of  $r_{\text{s}} + a$ . Since the ions have diameter  $a$  this corresponds to a rod radius  $r_0$  of  $r_0 = r_{\text{s}} + a/2$ . Of course, in this case  $r$  is a cylindrical and not a spherical radial coordinate.

The electrostatic interaction energy between two ions with charge  $z_i e_0$  and  $z_j e_0$ , is given by

$$V_{ij}^{\text{el}}(r) = k_{\text{B}}T \frac{z_i z_j \ell_{\text{B}}}{r} \quad \text{with} \quad \ell_{\text{B}} := \frac{e_0^2}{4\pi\epsilon_0\epsilon_{\text{r}}k_{\text{B}}T}, \quad (2)$$

where  $z_i$  is the valence of the  $i$  species and  $e_0$  the elemental charge. By definition the *Bjerrum length*  $\ell_{\text{B}}$  is the distance at which two unit charges have interaction energy  $k_{\text{B}}T$ . With the vacuum dielectric constant  $\epsilon_0 = 8.85 \times 10^{-12} \text{C}^2 \text{m}^{-2} \text{N}^{-1}$  and the dielectric coefficient  $\epsilon_{\text{r}} = 78.5$  applying to water at room temperature, one gets a Bjerrum length of approximately  $7.14 \text{ \AA}$ . The line charge density  $\lambda$  of the rod is modeled by placing unit charges along the rod axis at the distance  $b = e_0/\lambda$ . The number of charges along the rod per Bjerrum length is an important dimensionless measure of the line charge density and is often referred to as the Manning parameter:

$$\xi = \frac{\lambda \ell_{\text{B}}}{e_0} = \frac{\ell_{\text{B}}}{b}. \quad (3)$$

Its relevance lies in the fact that for  $\xi > 1$  the phenomenon of counterion ‘‘condensation’’ is observed [7].

Within the periodic boundary conditions employed during the simulations, the presence of such long-range

interactions poses both mathematical and technical difficulties. We use an efficient FFT accelerated Ewald sum, the P<sup>3</sup>M algorithm, which scales almost linearly with the number of charges [35, 36, 37].

The final step consists of explicitly mapping the parameters to a DNA system in aqueous solution. This affects ion diameter  $a$ , rod radius  $r_0$ , Bjerrum length  $\ell_{\text{B}}$  and line charge density  $\lambda$ . Our choice is presented in Table I.

We performed Molecular-Dynamics simulations of the rod-systems using a Langevin thermostat in order to drive the system into the canonical state [38]. The real-space and Fourier-space part of the electrostatic energy was used to check for equilibration. The presented observables originate from averaging over roughly 1500 independent configurations.

## HNC/MSA THEORY

The integral equation formalism is a well established statistical mechanical approach that has been shown to be reliable when it is applied to simple microscopic models of inhomogeneous fluids [39, 40]. A particularly successful integral equation theory for inhomogeneous, charged fluids is the so-called hypernetted-chain/mean spherical approximation (HNC/MSA) [25, 41, 42, 43]. The HNC/MSA theory for a model charged rod, immersed in an electrolyte, has been derived in the past [17, 18]. In this paper, we solve the HNC/MSA equation for an infinitely long, hard, charged cylinder of radius  $r_0$ , with uniform line charge density  $\lambda$ . The rod is immersed in a two-component restricted primitive model electrolyte (RPM), i.e., a fluid of charged hard spheres of diameter  $a$  with a centered point charge  $z_i e_0$ .

The fluid electroneutrality condition is

$$\sum_{m=1}^2 z_m \rho_m = 0, \quad (4)$$

where  $\rho_m$  is the bulk concentration of species  $m$ . In order to satisfy the necessary condition of zero electrical field at infinity, the rod charge is compensated by the charge induced in the fluid,  $\lambda'$ :

$$\lambda' \equiv 2\pi \int_{r_0+a/2}^{\infty} \rho_{\text{el}}(r) r dr = -\lambda, \quad \text{with} \quad \rho_{\text{el}}(r) \equiv e_0 \sum_{m=1}^2 z_m \rho_m(r). \quad (5)$$

The local concentration profile of the species  $m$  is denoted as  $\rho_m(r)$ . The solvent is taken as a dielectric continuum of dielectric constant  $\epsilon_{\text{r}}$ . For simplicity, rod and solvent are assumed to have the same dielectric constant, in order to avoid complications with dielectric boundaries.

It has long been recognized in physics that particles and fields are equivalent in the sense that both are defined through their interaction potentials. This simple fact has been applied in the past to derive, in a straightforward

manner, inhomogeneous integral equation theories from the Ornstein-Zernike (OZ) equation for homogeneous fluids [40, 44]. The homogeneous three-component OZ equation is

$$h_{ij}(\mathbf{r}_{21}) = c_{ij}(\mathbf{r}_{21}) + \sum_{m=1}^3 \rho_m \int h_{im}(\mathbf{r}_{23}) c_{mj}(\mathbf{r}_{13}) dv_3. \quad (6)$$

where  $h_{ij}(\mathbf{r}_{21})$  and  $c_{ij}(\mathbf{r}_{21})$  are the total and direct correlation functions, between particle 2 located at  $\mathbf{r}_2$  and particle 1 at  $\mathbf{r}_1$  of species  $i$  and  $j$ , respectively,  $\mathbf{r}_{21} \equiv \mathbf{r}_2 - \mathbf{r}_1$ .

In consequence, one can consider a particle of a fluid as a source of an external field or an external field as a particle of the fluid. Applying this simple idea to Eqn. (6), one can think of one of the species, say  $\alpha$ , as made of infinite cylindrical rods and the remaining two species as ions. In  $\alpha$ 's infinite dilution limit the cylinders are uncorrelated. Hence, letting  $\rho_\alpha \rightarrow 0$ , the Ornstein-Zernike equation for an ionic solution next to a charged cylinder reads

$$h_{\alpha j}(\mathbf{r}_{21}) = c_{\alpha j}(\mathbf{r}_{21}) + \sum_{m=1}^2 \rho_m \int h_{\alpha m}(\mathbf{r}_{23}) c_{mj}(\mathbf{r}_{13}) dv_3. \quad (7)$$

In the past, several approximations (or ‘‘closures’’) for the direct correlation function have been suggested. Two of them are:

$$\begin{aligned} \ln(g_{ij}(\mathbf{r}_{21})) &= -\beta V_{ij}(\mathbf{r}_{21}) + h_{ij}(\mathbf{r}_{21}) - c_{ij}(\mathbf{r}_{21}) \quad (8) \\ c_{ij}(\mathbf{r}_{21}) &= -\beta V_{ij}(\mathbf{r}_{21}). \quad (9) \end{aligned}$$

Eqn. (8) and Eqn. (9) are known as the hypernetted chain (HNC) equation and the mean spherical approximation (MSA), respectively;  $V_{ij}(\mathbf{r}_{21})$  is the direct interaction potential between species  $i$  and  $j$ , and  $\beta \equiv 1/k_B T$ .

If the HNC closure is used for the direct correlation function between the rod particle and the  $j$  species, equation (7) becomes

$$\begin{aligned} g_{\alpha j}(\mathbf{r}_{21}) &= \exp\{-\beta V_{\alpha j}(\mathbf{r}_{21}) \\ &+ \sum_{m=1}^2 \rho_m \int h_{\alpha m}(\mathbf{r}_{23}) c_{mj}(\mathbf{r}_{13}) dv_3\}, \quad (10) \end{aligned}$$

In this scheme, the two-particles correlation functions  $h_{\alpha j}(\mathbf{r}_{21})$  and  $c_{\alpha j}(\mathbf{r}_{21})$  correspond to the one-particle total and direct inhomogeneous correlation functions  $h_j(\mathbf{r})$  and  $c_j(\mathbf{r})$  for species  $j$  of a fluid under the influence of an external field produced by a rod particle. The local concentration for the  $j$  species is given by  $\rho_j(\mathbf{r}) = \rho_j g_j(\mathbf{r})$ , where  $g_j(\mathbf{r}) = h_j(\mathbf{r}) + 1$  is called the reduced concentration profile. Therefore, the charge concentration profile in Eqn. (5) is given by

$$\rho_{ei}(r) = \sum_{m=1}^2 z_m e_0 \rho_m g_m(r). \quad (11)$$

For this model the direct interaction potential between the rod and the  $j$  species of the fluid,  $V_j(r)$ , can be separated into two parts: the hard sphere-hard rod term  $V_j^*(r)$  and the electrostatic interaction potential  $V_j^{\text{el}}(r)$ . The first takes into account the fact that ions cannot penetrate or deform the cylinder

$$V_j^*(r) = \begin{cases} \infty & : 0 < r \leq r_0 + a/2 \\ 0 & : r > r_0 + a/2 \end{cases} \quad (12)$$

The second can be found from Gauss' law and is given by

$$-\beta V_j^{\text{el}}(r) = 2z_j \xi \ln(r) \quad (r > r_0). \quad (13)$$

In the MSA closure the homogeneous direct correlation function for a RPM electrolyte has an analytical expression. This function can be written as

$$c_{mj}(s) = -\beta V_{mj}^{\text{el}}(s) + z_m z_j c_d^{\text{sr}}(s) + c_s^{\text{hs}}(s). \quad (14)$$

In the first term appears the direct electric interaction potential between the species of the fluid, which is given by Eqn. (2), the second term is an electrical short range function and the third is the direct correlation function for a hard sphere fluid. When the MSA closure is used in the integral of Eqn. (11), one obtains the HNC/MSA equation for an ionic fluid next to a charged rod. Taking advantage of the cylindrical geometry and the fact that the direct correlation function between the ions depends only on their relative distance  $s \equiv |\mathbf{r}_1 - \mathbf{r}_3|$ , Eqn. (11) can after some algebra be written as [17, 18]

$$g_j(r) = \exp\{-\beta(z_j e_0 \psi(r) + J_j(r))\}, \quad (15)$$

where  $\psi(r)$  is the mean electrostatic potential

$$\begin{aligned} -\beta e_0 \psi(r) &= 2\xi \ln(r) \\ &+ 2\pi \ell_B \int_{r_0+a/2}^{\infty} \rho_{cd}(y) \ln((r^2 + y^2 + |r^2 - y^2|)/2) y dy. \end{aligned} \quad (16)$$

The  $J_j(r)$  terms are integrals of the short range terms of the direct correlation function

$$\begin{aligned} -\beta J_j(r) &= \rho A(r) + z_j \int_{r_0+a/2}^{\infty} \rho_{cd}(y) L(r, y) dy \\ &+ \int_{r_0+a/2}^{\infty} \rho_{cs} K(r, y) dy, \end{aligned} \quad (18)$$

with

$$\begin{aligned} \rho &= \sum_{m=1}^2 \rho_m, \\ \rho_{cs}(y) &= \sum_{m=1}^2 \rho_m h_m(y), \\ \rho_{cd}(y) &= \sum_{m=1}^2 z_m \rho_m h_m(y), \end{aligned}$$

and

$$L(r, y) = 4y \int_0^{\phi_{max}} d\phi \int_0^{z_{max}} c_d^{sr}(s) dz$$

$$K(r, y) = 4y \int_0^{\phi_{max}} d\phi \int_0^{z_{max}} c_s^{hs}(s) dz$$

$$A(r) = - \int_0^{r_0+a/2} K(r, y) dy$$

where  $s^2 = z^2 + r^2 + y^2 - 2ry \cos \phi$ . In the limit  $a \rightarrow 0$  of point ions,  $c_d^{sr}(s)$  and  $c_s^{hs}(s) \rightarrow 0$ . Thus  $J_j(r) \rightarrow 0$  [17] and Eqn. (15) becomes

$$g_m(r) = \exp \{ -\beta z_m e_0 \psi(r) \}, \quad (19)$$

where  $\psi(r)$  is given by Eqn. (17), which is the solution of the well known PB differential equation for point ions around a charged cylindrical electrode, i.e.,

$$\frac{1}{r} \frac{d\psi(r)}{dr} + \frac{d^2\psi(r)}{dr^2} = -\frac{e_0}{\epsilon_0 \epsilon_r} \sum_{m=1}^2 z_m \rho_m \exp \{ -\beta z_m e_0 \psi(r) \}. \quad (20)$$

Therefore, the integral equation version of the Poisson-Boltzmann differential equation is [17]

$$g_j(r) = \exp \{ 2z_j \xi \ln(r) \} + 2z_j \pi \ell_B \int_{r_0+a/2}^{\infty} \rho_{cd}(y) \ln((r^2 + y^2 + |r^2 - y^2|)/2) y dy \quad (21)$$

which is also the HNC/MSA equation in the point ions limit. The differences between these two theories are due to the ionic size correlations which are partially taken into account in HNC/MSA theory but which are ignored in the PB equation. In the past, it has been shown that the size effects become important for strong field interaction, poly-valent ions and high salt concentration [18].

The HNC/MSA and PB integral equations are numerically solved with efficient finite element methods [16, 45]. The solution of Eqn. (15) takes one minute in a R12000 processor of an SGI machine. In our theoretical calculation we use the same input parameters as in our MD calculations. The salt concentration is obtained through

$$\rho_s = N_s / L_b^3, \quad (23)$$

where  $N_s$  is the number of salt molecules used in the simulation. Nevertheless, we have to point out the differences in the short range interaction used in both models. While in HNC/MSA we use hard particles, the MD for technical reasons uses the potential from eq. 1, which has some surface softness. This results in an effective excluded volume, whose actual value depends on the interaction strength. At an interaction energy of  $k_B T$  the particle diameter is  $a$ . However, if the particles attract each other strongly, they can come closer to each other.

parameter	symbol	value	value in LJ units
ion diameter	$a$	4.25 Å	$a$
ion valence	$z$	2	2
rod radius	$r_0$	7.86 Å	1.85 $a$
line charge density (DNA)	$\lambda$	$-e_0/1.7$ Å	$-2.5 e_0/a$
Bjerrum length (water)	$\ell_B$	7.14 Å	1.68 $a$
Manning parameter	$\xi$	4.2	4.2
box size	$L_b$	122.4 Å	28.8 $a$
corresponding cell radius	$R$	69.1 Å	16.2 $a$
temperature	$T$	298 K	$\epsilon/k_B$

TABLE I: System parameters for the DNA simulations.

## RESULTS

We will discuss the results in terms of the mean electrostatic potential,  $\psi(r)$ , the local concentration profiles,  $g_m(r)$ , and the integrated charge distribution function

$$P(r) = \frac{1}{|\lambda|} \int_{r_0}^r d\bar{r} 2\pi\bar{r} \rho_{el}(\bar{r}). \quad (24)$$

Figure 2 shows the HNC/MSA and MD results for  $P(r)$  and  $\psi(r)$ , for five rod-systems, for which the line charge density, and thereby the Manning parameter, has been successively increased. One system has a smaller Manning parameter than DNA and three a larger. All systems have a Debye screening length which is much smaller than the Manning radius of the corresponding salt free system. According to the observations of Ref. [9] this means that the concept of Manning “condensation” is no longer meaningful. The rod charge is compensated by salt screening. According to simple PB theory, no remarkable features are to be expected in the bulk solution. Contrary to that, however, in Fig. 2a  $P(r)$  shows overcharging, i.e., the rod charge is over-compensated at a certain distance from the rod. For a given salt concentration the degree of overcharging is increased as the charge density increases. No overcharging saturation point is observed, at least for physical charge densities. While in Fig. 2a overcharging is present even for a very low charge density, such as  $\sigma = 0.095 \text{C/m}^2$  our HNC/MSA calculations show overcharging for even lower rod charge densities. We will come back to this point later. In Fig. 2a, the maximum of overcharging is closer to the rod’s surface as  $\sigma$  increases. This effect has implication for the location of the so-called  $\zeta$ -potential, in electrophoresis experiments [31]. As pointed out before [18, 23], overcharging implies a change of direction in the local electrical field. Our MD and HNC/MSA results are consistent with this fact, as shown in Fig. 2b, where a minimum in  $\psi(r)$  is observed. The value of  $r$  at the minimum of  $\psi(r)$ , i.e., where the electrical field is zero, coincides with that at which  $P(r) = 1$ , as it should.

Integral equation theories give much more reliable re-

$\xi$	$\zeta_{\text{LPB}}$ [mV]	$\zeta_{\text{PB}}$ [mV]	$\zeta_{\text{HNC}}$ [mV]	$\zeta_{\text{MD}}$ [mV]
0	0	0	0	0
1.05	10.52	10.28	6.262	9.116
2.1	21.04	19.48	10.99	14.62
4.2	42.09	33.32	14.27	16.25
6.3	63.13	42.96	11.08	13.80
8.4	84.17	50.16	3.771	9.263
10.5	105.2	56.03	-6.219	3.675

TABLE II:  $\zeta$ -potential of a DNA-sized rod (see Tab. I) immersed into a 0.49 M electrolyte of 2:2 salt as a function of its Manning parameter  $\xi$ . The four predictions are from linear PB theory, PB theory, hypernetted-chain theory and MD simulation. The error in the latter is estimated to be of the order of 2%. Figure 5 visualizes the data.

sults than Poisson-Boltzmann at high salt concentrations, poly-valent ions and/or for fluids under the influence of strong external fields. This is because they partially take into account correlations due to the ionic size, which PB theory ignores. It can be seen that the HNC/MSA theory indeed correctly predicts the occurrence of overcharging, although it overestimates its amount. The qualitative agreement between the HNC/MSA and MD results is excellent. The quantitative agreement is fair and particularly good for the DNA calculation. In the next section we will discuss the disagreement seen between the HNC/MSA and MD results, for high and low cylinder charge densities.

For a given constant value of the Manning parameter, cylindrical macroions with different diameters will produce different EDL structures. In Figure 3, HNC/MSA results for rods with the same value of  $\xi$  but different diameters show different charge distributions  $P(r)$ . This illustrates the simple fact that the Manning parameter  $\xi$  alone is not sufficient to specify the ionic structure around cylindrical macroions. Since the ionic structure depends directly on the field strength, it is often better to use the cylinder's surface charge density  $\sigma$ , which is a direct measure of the electrical field that penetrates into the solution. Note, however, that  $\xi$  and  $\sigma$  are simply related by  $\xi = 2\pi r_0 \sigma \ell_B / e_0$ .

In Figs. 4a and 4b we show HNC/MSA and MD reduced concentration profiles for  $\sigma = 0.190 \text{ C/m}^2$  ( $\xi = 4.2$ ) and  $\sigma = 0.49 \text{ C/m}^2$  ( $\xi = 10.5$ ), respectively, whereas all the other parameters are the same as in Fig. 2. The value of  $r$  at the maximum of  $P(r)$  matches with that where  $g_+(r) = g_-(r)$ , at least for symmetric electrolytes. Therefore the later oscillation in the local concentration profiles, show the attraction (repulsion) to coions (counterions), due to a change in direction of the effective electrical field. On the other hand, concentration profile oscillations are a consequence of the ionic size correlations. Hence, overcharging results of electrostatic attraction and size correlations.

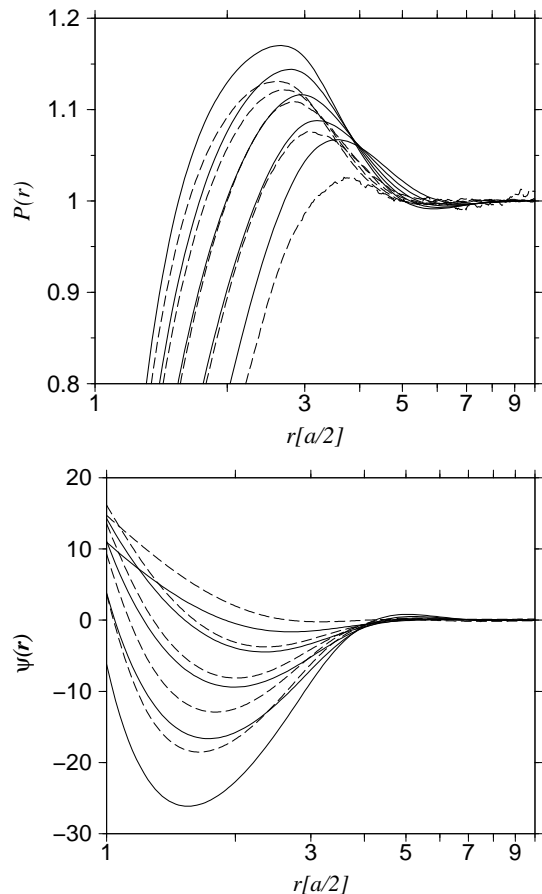


FIG. 2: (a) Charge distribution function  $P(r)$  and (b) mean electrostatic potential  $\psi(r)$  for the parameters from Tab. I. The electrolyte is a 2:2 salt of concentration 0.49 M. The distance  $r$  is measured with respect to the cylinder surface in units of the ionic radius. The solid and dashed lines correspond to the HNC/MSA and MD calculations, respectively. The different curves are for different values of the Manning parameter,  $\xi = 2.1, 4.2, 6.3, 8.4, 10.5$ , which correspond to surface charge densities of  $\sigma = 0.095, 0.190, 0.286, 0.381, 0.476 \text{ C/m}^2$ , respectively. In  $P(r)$ , the surface charge density increases from bottom to top, whereas in the mean electrostatic potential it increases from top to bottom. The value  $\xi = 4.2$  ( $\sigma = 0.190 \text{ C/m}^2$ ) corresponds to DNA.

The first maximum seen in the coion reduced concentration profile implies a coion concentration above its bulk value and indicates that the local electric field is attractive to coions. It is also observed that HNC/MSA overestimates the contact value of the distribution function with respect to molecular dynamics predictions. The overestimation of HNC/MSA can be associated with two facts: (i) the difference in excluded volume used in both models; and (ii) HNC/MSA theory does not take into account all the size and charge correlations.

Another important phenomenon is indicated by the behavior of the mean electrostatic potential in Fig. 2b. It concerns the value of this potential at the distance of

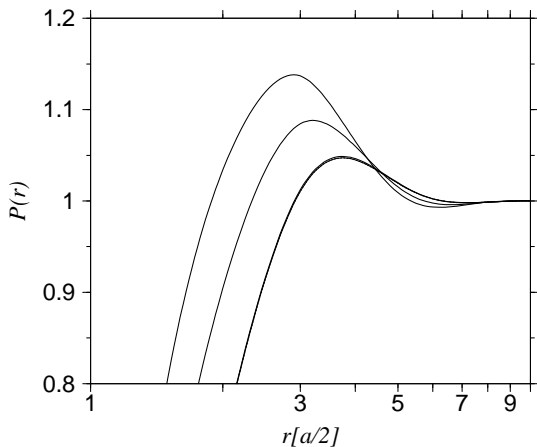


FIG. 3: Charge distribution function from HNC/MSA, for a RPM electrolyte next to a charged cylinder. The distance  $r$  is measured with respect to the cylinder surface in units of the ionic radius. The electrolyte is a 2:2, 0.49 M salt. The results correspond to different cylinder radii, whereas the Manning parameter has been held constant at  $\xi = 4.2$ . From top to bottom the cylinder radii are  $r_0 = 3.86, 7.86, 110, 1200$  Å, which correspond to the surface charge densities  $\sigma = 0.388, 0.190, 10^{-2}, 10^{-3}$  C/m<sup>2</sup>, respectively. The curves for  $r_0 = 110$  Å and  $r_0 = 1200$  Å are indistinguishable on this scale.

closest approach between ions and the rod,

$$\zeta = \psi(r_0 + a/2), \quad (25)$$

which can be identified with the zeta-potential of electrophoresis and which is of importance in the computation of electrophoretic mobilities [31, 46]. In the PB theory for a charged rod immersed into an ionic solution, and its linearized version,  $\zeta$  depends monotonically on  $\xi$  [18]. However, Fig. 2 shows that, in the presence of overcharging,  $\psi(r)$  can become negative. This calls the monotonic relation between  $\zeta$  and  $\xi$  into question. Table II summarizes various predictions for the  $\zeta$ -potential as a function of Manning parameter together with results from the molecular dynamics simulations. A graphical illustration is given in Fig. 5.

Indeed,  $\zeta$  is found to first increase with  $\xi$ , but from a certain value on it decreases and would finally even become negative. Note that this would reverse the drift direction in electrophoresis measurements, as first predicted by Gonzales-Tovar *et al.*[18] and recently demonstrated, for spherical macroions, by Lozada-Cassou *et al.*[31]. While nonlinear and linearized PB theory coincide with the data and with each other for small Manning parameter, they completely fail to predict the back-bending, which already sets in at comparatively small values of  $\xi$ . The HNC/MSA theory captures this effect, but it underestimates the value of the potential. However, comparisons for the  $\zeta$ -potential, as a function of  $\sigma$ , between HNC/MSA and MC simulations for planar and spherical hard, charged macroions, immersed into a RPM

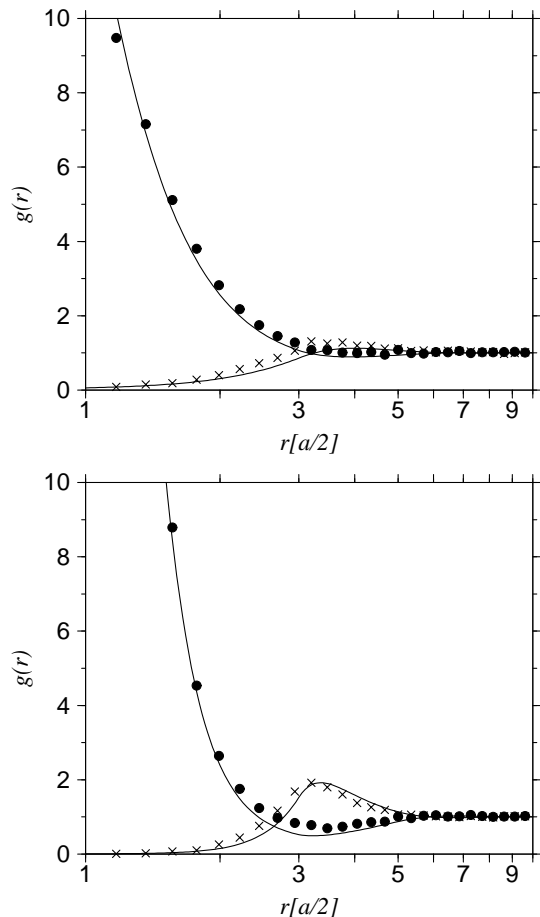


FIG. 4: Reduced concentration profiles  $g_i(r)$  for an electrolyte next to a charged cylinder. The electrolyte is a 2:2, 0.49 M salt. The distance  $r$  is measured with respect to the cylinder surface in units of the ionic radius. The system parameters are given in Tab. I. Fig. 4a shows the results corresponding to  $\xi = 4.2$  ( $\sigma = 0.190$  C/m<sup>2</sup>) and Fig. 4b the results for  $\xi = 10.5$  ( $\sigma = 0.49$  C/m<sup>2</sup>). The dots and crosses are the MD distribution functions for counterions and coions, respectively. The solid lines are the results from HNC/MSA.

electrolyte, have been made in the past [25, 43, 47]. For these two geometries, for 1:1 electrolytes and for 2:2, at around 0.5 M, as in our Fig. 5, the HNC/MSA-MC agreement is excellent. The disagreement seen in Fig. 5 can be related to the different short-range potentials used in our MD and HNC/MSA calculations, which gives for the MD not a sharply defined ion-cylinder contact. This is important, since the  $\zeta$ -potential is evaluated exactly there. For planar and spherical macroions, PB  $\zeta$  vs. charge curves are also above the HNC/MSA and MC curves, which is consistent with our present observations.

For a given rod charge and diameter, for any electrolyte solution parameters, a higher  $\zeta$ -potential always implies a lower counterions adsorption [18]. A soft-repulsive short-range potential, as in our MD calculations, allows the counterions to get closer to the rod. This produces a

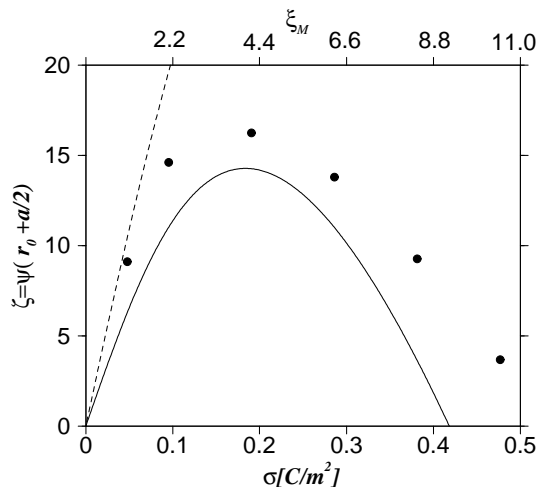


FIG. 5: Zeta potential  $\zeta \equiv \psi(r_0 + a/2)$  as a function of surface charge density  $\sigma$ , for a cylinder immersed in a 0.49 M, 2:2 electrolyte. The model parameters are given in Tab. I. The dotted line is the prediction of PB theory, the dots are the MD results and the solid line is the results from HNC/MSA calculations.

higher  $\zeta$ -potential in the MD simulation when compared to the HNC/MSA results. In the case of the PB theory, the neglect of the ionic-size correlations allows a higher density of counterions next to the rod, which in turn can never lead to overcharging.

In all cases, the HNC/MSA qualitative agreement with MD is very good. The success of HNC/MSA theory indicates that local ion-size correlations are responsible for both phenomena. As it is concluded by Lozada-Cassou and Jiménez-Ángeles in ref. [48], overcharging increases with an increase of the system excluded volume: i.e., higher ionic size and/or concentration. If size correlations are not considered (as in PB theory) or are negligible, overcharging does not occur, even for divalent ions. On the other hand, overcharging can occur in a high excluded volume system even for monovalent ions. To illustrate this fact we have simulated two systems, for which the distance of closest approach to the charged rod is in both cases 9.98 Å, hence DNA-like. The first rod system has a charge parameter of  $\xi = 4.2$  ( $\sigma = 0.240 \text{ C/m}^2$ ) and is immersed in a 1.0 Molar 1:1 electrolyte solution with ions of diameter  $a = 7.4 \text{ \AA}$ . The second rod system has an even higher charge parameter of  $\xi = 10.5$  ( $\sigma = 0.40 \text{ C/m}^2$ ) and is immersed in a 0.5 Molar 2:2 electrolyte, but, this time, the diameter is only  $a = 1.0 \text{ \AA}$ . The results are shown in Fig. 6, where the charge distribution function is plotted. Contrary to the general believe, the system with the large monovalent ions shows overcharging, both in the HNC/MSA and the MD results, and the location of the peaks coincide, whereas we see small differences in the height. Further, strikingly, the system with small divalent ions shows no sign of overcharging, although the charge

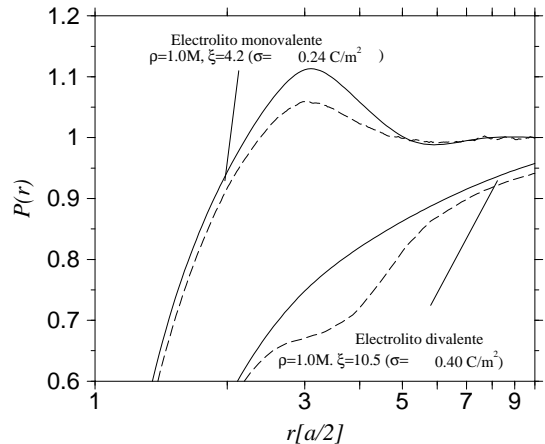


FIG. 6: Charge distribution function from HNC/MSA (solid lines) and MD (dotted lines), for a RPM electrolyte next to a charged cylinder to which the ions have a distance of closest approach of 9.98 Å. The distance  $r$  is measured with respect to the cylinder surface in units of the ionic radius. In this plot a comparison between a low and a high excluded volume systems is presented. The system where overcharging occurs corresponds to a monovalent electrolyte with  $\rho = 1.0 \text{ M}$ ,  $\xi = 4.2$  ( $\sigma = 0.240 \text{ C/m}^2$ ), and large ions ( $a = 7.4 \text{ \AA}$ ). The system where overcharging is not observed corresponds to a divalent electrolyte with  $\rho = 0.5 \text{ M}$ ,  $\xi = 10.5$  ( $\sigma = 0.40 \text{ C/m}^2$ ), and small ions ( $a = 1.0 \text{ \AA}$ ).

parameter for this system is even higher. The shoulder in the distribution of the MD simulation indicates that the second ionic layer is almost neutral. A possible explanation is the following: The small ions have an energy of attraction of almost  $30k_B T$ , hence the salt is actually present in the form of little overall neutral salt clusters. This is supported by visual inspection of the MD configurations. These mostly neutral clusters are polarizable and hence tend to accumulate in the large field gradient surrounding the rod. The free counterions left can come only from the rods charge and can in no way lead to an overcharging. A key prerequisite for this scenario is that the interaction energy between ions exceeds the interaction between ions and the rod. Also consistent is, that the HNC/MSA calculation as well shows the vanishing of the overcharging.

Finally, one might ask the question of how the effect of overcharging depends on salt concentration. Obviously there can not be any overcharging in the absence of salt, since then even a complete “condensation” of all ions would merely neutralize the rod. However, it is not clear from the beginning whether an addition of just *some* salt will immediately lead to overcharging. Figure 7 shows HNC/MSA and MD distribution functions  $P(r)$  and mean electrostatic potentials  $\psi(r)$  for a DNA-sized and charged rod, immersed into a 2:2 electrolyte, for varying salt concentrations. The phenomenon



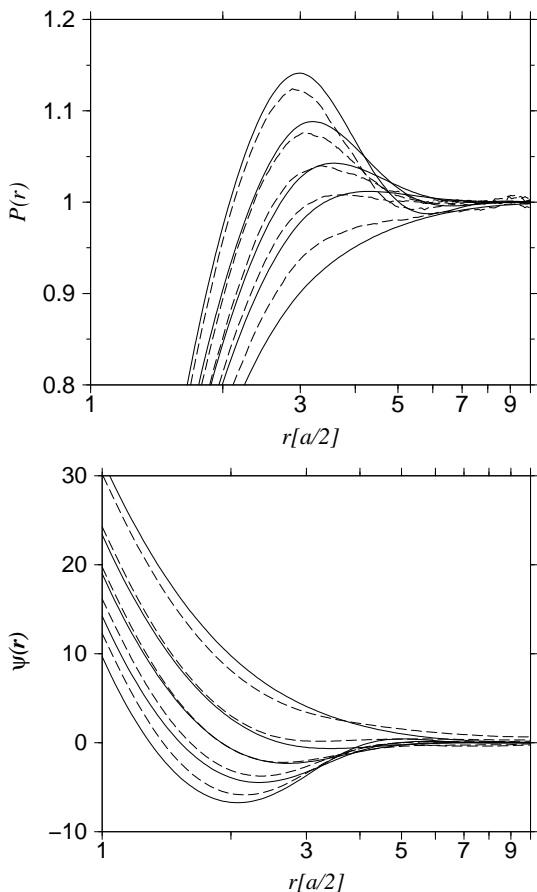


FIG. 7: Charge distribution function  $P(r)$  (left) and mean electrostatic potential  $\psi(r)$  (right) results, for the system from Tab. I with Manning parameter  $\xi = 4.2$ . The distance  $r$  is measured with respect to the cylinder surface in units of the ionic radius. The line styles have the same meaning as in Fig. 2. The curves correspond to different salt concentration,  $\rho_s = 0.12, 0.24, 0.34, 0.49, 0.68$  M. In the charge distribution function the salt content increases from bottom to top, in the mean electrostatic potential it increases from top to bottom.

of overcharging is indeed observed, but only at sufficiently high salt concentration. These results are consistent with the fact that higher electrolyte concentration increases the excluded volume, thus increases overcharging [48]. Therefore, as proposed in Ref. [48], higher excluded volume implies higher overcharging. This may be also illustrated by defining  $r_1$  to be the radius at which overcharging sets in, i.e.,

$$r_1 = \min \{r : P(r) = 1\}. \quad (26)$$

Fig. 8 illustrates the measured  $r_1$  together with a hypernetted-chain prediction as a function of salt concentration  $\rho_s$ . Clearly,  $r_1$  must increase with decreasing  $\rho_s$ , since overcharging is reduced and consequently the size of the charge-compensating layer must increase. In fact, hypernetted-chain theory predicts that  $r_1(\rho_s)$  diverges at some *finite* density  $\rho_s^\infty \approx 0.18$  mol/l corresponding to a

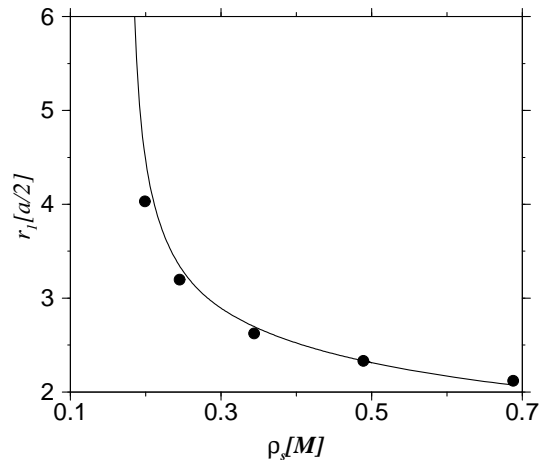


FIG. 8: Radius  $r_1$  from Eqn. (26) at which overcharging sets in, for a DNA-sized and -charged cylinder ( $r_0 = 7.86\text{\AA}$  and  $\sigma = 0.190$  C/m<sup>2</sup>), as a function of salt concentration  $\rho_s$ . The distance  $r_1$  is measured with respect to the cylinder surface in units of the ionic radius. The dots are the results of molecular dynamics simulations while the solid line is the prediction of HNC/MSA.

salt Debye length of  $3.59\text{\AA}$ , or roughly 200 salt molecules within the simulation box. For the lower concentrations, the simulated  $r_1$  values lie below the hypernetted-chain prediction, but this is not a feature generally to be expected. In Fig. 7 it can be seen that the stronger overcharging in hypernetted-chain theory should normally lead to a value of  $r_1$  smaller than in the simulation. But with decreasing density the finite radius of the simulation cell becomes relevant. Indeed, zero-salt distribution functions reach the value 1 at the cell boundary, and not at infinity. A reduction of the amount of added salt at fixed cell radius must necessarily lead to values of  $r_1$  smaller than the hypernetted chain prediction for the bulk, since within a finite cell  $r_1$  cannot diverge. On the other hand, for technical reasons, the MD cell radius can not be increased indefinitely. In any case, our MD results have not been able to unambiguously detect overcharging at densities equal to or lower than 0.2 M, which is in excellent agreement with the HNC/MSA prediction for the minimum amount of salt needed to induce overcharging. From Figs. (7) and (8) it is clear that excluded volume effects determine the occurrence of overcharging, as proposed by some of us [48].

## CONCLUSION

Theoretical and numerical studies of stiff linear polyelectrolytes, immersed into a 2:2 RPM electrolyte have been presented. The qualitative agreement between the MD and HNC/MSA results is excellent. For the particular case of DNA parameters, there is also a very

good quantitative agreement. We argued that the better agreement in the planar and spherical case reported in Refs. [25, 43, 47] is most probably due to an implementation of the short range interactions that is identical to the theoretical model and not merely very close. At low salt concentrations the difference between a finite cell used in simulations and the  $R = \infty$  system used in the HNC/MSA calculations becomes important. Also, the macroion and ions electrical fields are much less screened and, hence, the charge correlations become more important [2]. Both these points are responsible for the disagreement between theory and simulations at low salt. While the former can in principle be resolved by increasing the size of the simulation cell, the latter can be addressed by the three point extension HNC/MSA theory [17, 40], which gives a better account of these correlations [48].

In the past the HNC/MSA theory for an electrolyte next to a charged rod has been derived [17] and applied [18] to simple DNA models. In this paper we have shown this theory to be qualitatively correct. In particular, for DNA parameters the quantitative agreement is excellent. To the best of our knowledge, in Gonzales-Tovar *et al.*[18] overcharging has first been predicted theoretically. It was pointed out that this should entail an electrophoresis mobility reversal. In the PB theory the  $\zeta$ -potential as a function of the cylinder charge density is a monotonic function, while in the HNC/MSA theory it is not. In this paper we have shown the HNC/MSA prediction to be in agreement with MD calculations. This non-monotonic behavior of the  $\zeta$ -potential has important implications in electrophoresis calculations. The standard electrophoresis theory [21, 22] is based on the PB prediction for  $\zeta$  and, hence, important differences should be found if the HNC/MSA theory is applied to the electrophoresis problem.

Recently, Lozada-Cassou *et al.*[31] extended the electrophoresis theory to include ionic size effects, through the HNC/MSA theory. It was applied to spherical macroions. A mobility reversal and a very non-linear behavior of the mobility, as a function of the  $\zeta$ -potential, were predicted. These predictions were found to be in agreement with experimental results. Contrary to the standard electrophoresis theory, the mobility was shown to be non-universal. This is due, precisely, to the non-monotonic behavior of the  $\zeta$ -potential. The HNC/MSA and MC simulations for spherical and planar macroions do not show a maximum in  $\zeta(\sigma)$  as pronounced as that reported here for the cylindrical geometry. Therefore, we believe that our HNC/MSA and MD results are particularly relevant.

In view of the qualitative agreement between HNC/MSA and MD and the quantitative and qualitative disagreement of these with Poisson-Boltzmann theory, we conclude that for concentrated and divalent electrolytes, influenced by charged polyelectrolytes, the size correla-

tions must be taken properly into account to describe the cylindrical double layer. Our MD results clearly indicate that overcharging strongly depends on the system excluded volume, as proposed by some of us [48]. While maximum overcharging does not seem to have a limit, the minimum conditions to have overcharging depend on many different ways in which ionic charge, size and concentration, and surface charge density participate in a system, as we showed in Figs. (2), (6) and (7)

## ACKNOWLEDGMENTS

CH and MLC wish to thank W. Gelbart and The Institute for Theoretical Physics, University of California at Santa Barbara, where this project was started, for their hospitality. MLC which to thank C. Holm and K. Kremer for their hospitality at Mainz. FJA and MLC gratefully acknowledge the financial support of INDUSTRIAS NEGROMEX. CH and MD acknowledge a large computer time grant hkf06 from NIC Jülich and financial support by the German Science foundation.

- 
- [1] Barrat J. L.; Joanny J. F. *Adv. Chem. Phys.* **1996**, *94*, 1.
  - [2] Lozada-Cassou M.; Díaz-Herrera E. *J. Chem. Phys.* **1990**, *93*, 1386 .
  - [3] Sánchez J. E.; Lozada-Cassou M. *Chem. Phys. Letts.* **1992** *190*, 202 .
  - [4] Jiménez-Ángeles F.; Messina R.; Holm C.; Lozada-Cassou M., *to appear elsewhere*.
  - [5] Alfrey T.; Berg P.; Morawetz H. J. *J. Polym. Sci.* **1951**, *7*, 543.
  - [6] Fuoss R. M.; Katchalsky A.; Lifson S. *Proc. Natl. Acad. Sci. USA* **1951**, *37*, 579.
  - [7] Manning G.; *J. Chem. Phys.* **1969**, *51*, 924.
  - [8] Oosawa F. *Polyelectrolytes*, Marcel Dekker: New York, 1971.
  - [9] Deserno M.; Holm C.; May S. *Macromolecules* **2000**, *33*, 199.
  - [10] Bloomfield V. *Biopolymers* **1991** *31*, 1471 .
  - [11] Valleau J. P.; Ivkov R.; Torrie G. M. *J. Chem. Phys.* **1991**, *95*, 520.
  - [12] Nilsson L. G.; Guldbrand L.; and Nordenskiöld L. *Mol. Phys.* **1991**, *72*, 177.
  - [13] Lyubartsev A. P.; Tang J. X.; Janmey P. A.; Nordenskiöld L. *Phys. Rev. Lett.* **1998**, *81*, 5465.
  - [14] Lozada-Cassou M.; Henderson D. *Chem. Phys. Lett.* **1986**, *127*, 392.
  - [15] Kjellander R.; Marcelja S. *J. Phys. Chem.* **1986**, *90*, 1230.
  - [16] Lozada-Cassou M.; Díaz-Herrera E. *J. Chem. Phys.* **1990**, *92*, 1194.
  - [17] Lozada-Cassou M. *J. Phys. Chem.* **1983**, *87*, 3279.
  - [18] Gonzales-Tovar E.; Lozada-Cassou M.; Henderson D. *J. Chem. Phys.* **1985**, *83*, 361.

- [19] Greberg H.; Kjellander R. *J. Chem. Phys.* **1998**, *108*, 2940.
- [20] Hidalgo-Álvarez R.; *et. al.*, *Adv. Colloid Interface Sci.* **1996**, *67*, 1, review article.
- [21] Wiersema P. H.; Leob A. L.; J. Th. G. Overbeek *J. Colloid Interface Sci.* **1966**, *22*, 78.
- [22] O'Brien R. W.; White L. R. *J. Chem. Soc., Faraday Trans. 2* **1978**, *74*, 1607.
- [23] Torrie G. M.; Valleau J. P. *J. Chem. Phys.* **1980**, *73*, 5807.
- [24] Vlachy V.; Haymet A. O. J. *J. Chem. Phys.* **1986**, *84*, 5874.
- [25] Degève L.; Lozada-Cassou M.; Sánchez E.; González-Tovar E. *J. Chem. Phys.* **1993**, *98*, 8905.
- [26] Degève L.; Lozada-Cassou M.; *Mol. Phys.* **1995**, *86*, 759.
- [27] U. P. Strauss, N. L. Gershfeld, and H. Spiera, *J. Am. Chem. Soc.* **76**, 5909 (1954).
- [28] Elimelech M.; O'Melia C. R. *Colloids Surf.* **1990**, *44*, 165.
- [29] Wang Y.; Kimura K.; Huang Q.; Dubin P. L. *Macromolecules* **1999**, *32*, 7128.
- [30] Huang Q. R.; Dubin P. L.; Moorefield C. N.; Newkome G. R. *J. Phys. Chem. B* **2000**, *104*, 898.
- [31] Lozada-Cassou M.; González-Tovar E.; Olivares W. *Phys. Rev. E* **1999**, *60*, R17.
- [32] Shklovskii B. I.; *Phys. Rev. E* **1999**, *60*, 5802.
- [33] Nguyen T. T.; Yu Grosberg A.; Shklovskii B. I.; *Phys. Rev. Lett.* **2000**, *85*, 1568.
- [34] Frenkel D.; Smit B. *Understanding Molecular Simulation*, Academic Press: San Diego, 1996.
- [35] Deserno M.; Holm C. *J. Chem. Phys.* **1998** *109*, 7678.
- [36] Deserno M.; Holm C. *J. Chem. Phys.* **1998**, *109*, 7694.
- [37] Hockney R. W.; Eastwood J. W. *Computer Simulation Using Particles*, IOP: London, 1988.
- [38] Grest G. S.; Kremer K. *Phys. Rev. A* **1986**, *33*, 3628.
- [39] Henderson D. In *Fundamentals of inhomogeneous fluids* Marcel Dekker, Inc., Edited by D. Henderson 1992; Chap. 4.
- [40] Lozada-Cassou M. In *Fundamentals of inhomogeneous fluids*, Marcel Dekker, Inc., Edited by D. Henderson 1992; Chap. 8.
- [41] Lozada-Cassou M.; Olivares W.; Sulbarán B. *Phys. Rev. E* **1996**, *53*, 522.
- [42] Yu J.; Degève L.; Lozada-Cassou M. *Phys. Rev. Lett.* **1997**, *79*, 3656.
- [43] Degève L.; Lozada-Cassou M. *Phys. Rev. E* **1998**, *57*, 2978.
- [44] Lozada-Cassou M. *J. Chem. Phys.* **1981**, *75*, 1412; **1982**, *77*, 5258.
- [45] Mier y Terán L.; Díaz-Herrera E.; Lozada-Cassou M.; Saavedra-Barrera R. *J. Comput. Phys.* **1989**, *84*, 326 .
- [46] Hunter R. J.; *Foundations of Colloid Science, Volume 1*, Oxford Science Publications, Clarendon Press: Oxford, 1987.
- [47] Lozada-Cassou M.; Saavedra-Barrera R.; Henderson D. *J. Chem. Phys.* **1982**, *77*, 5150; Lozada-Cassou M.; Henderson D. *J. Phys. Chem.* **1983**, *87*, 2821.
- [48] Lozada-Cassou M.; Jiménez-Ángeles F. *to appear elsewhere. (cond-matt/0105043)*